TESLA SPENT BEAM LINES

R.Brinkmann[1], R.Glantz[1], E.Merker[2], I.Yazynin[2]

[1]Deutsches Elektronen-Synchrotron DESY, Hamburg
[2] SRC Institute for High Energy Physics, 142284 Protvino, Moscow region, Russian Federation

Introduction

High energy and large intensity of beams in the linear collider TESLA [1] require a careful study of how to dispose both electron and positron beams after collision. To minimize uncontrollable activation of the collider equipment the beams are transferred to a dump foreseen for this purpose. To exclude the local overheating of the water dumps due to the high power of the beams (2×10^9 W in the pulse and $\approx 8\text{x}10^6$ W on average) the last should be distributed on a area not less than 30 cm^2 at the dump input [2].

The important feature of the TESLA project is that a new type of a positrons source will be used. The positrons are generated in a conversion target on which γ-radiation emitted by spent electrons in a wiggler is stricken. To provide the required intensity of the positrons not less than 70 % of the colliding electrons must be used. To ensure the necessary positron beam emittance the spot size of the γ-radiation on the target should not exceed 0.7 mm [3].

The choice of the transfer line structure for the electron beam from the extraction system up to dump, the definition of electromagnetic elements and the beam parameters are considered.

THE SPENT BEAM PROPERTIES

A very important consequence of the beams colliding in the intersection point (IP) is the significant beam parameters changing. In Fig.1, 2 the distributions on the transverse phase planes and in Fig.3 the energy spread of the particles after the interaction obtained using the simulation code developed by Brinkmann [4] are given. This data show that the curve limiting the area occupied by the beam, especially in the horizontal phase plane essentially differs from an ellipse and the particles energy distribution is unsymmetrical with a long tail in the small energies range. The results of the simulations were stored in a file of 12000 particles coordinates in a six-dimensional phase space and serve as the initial date for the further studies. Using them the statistical parameters in different points of the channel can be determined as follows [5]:

$$\varepsilon_x = \sqrt{\overline{x^2}\cdot\overline{x'^2} - \overline{xx'}^2}, \quad \beta_x = \frac{\overline{x^2}}{\varepsilon_x}, \quad \alpha_x = -\frac{\overline{xx'}}{\varepsilon_x}, \qquad (1)$$

where: ε is the statistical emittance, β, α are the statistical parameters of the equivalent phase ellipse of the beam, x and x' are the corresponding coordinates of the particles.

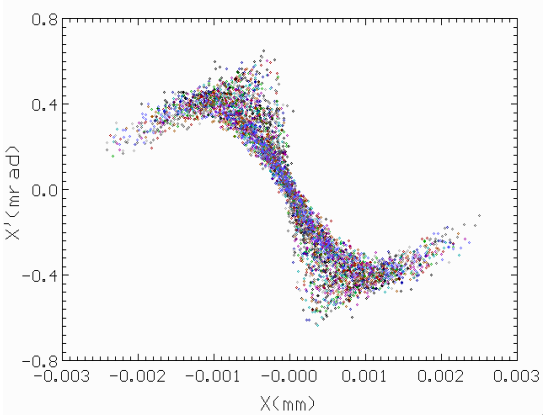

Fig.1: Horizontal phase plane in IP.

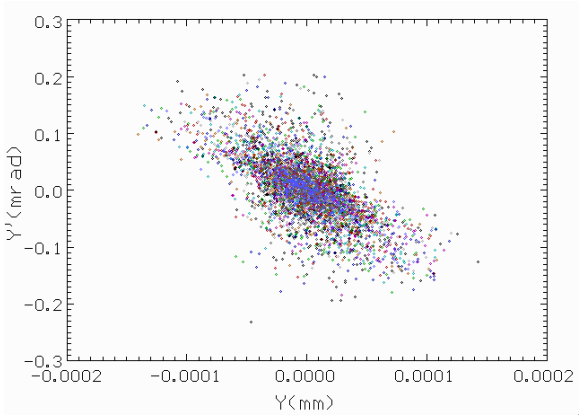

Fig.2: Vertical phase plane in IP.

In Table 1 for comparison the beam parameters in IP before and after the collision are presented. One can see the appreciable decreasing of the average particles energy because of the beamstrahlung and the

growth of the transverse emittances, especially in the horizontal plane caused by the angular divergence increasing due the beam - beam interaction.

	Units	input IP	output IP
Hor. Emittance ε_x	[10^{-11}m]	2.8	12.8
Ver. Emittance ε_y	[10^{-13}m]	5	13.2
Hor. β_x	[mm]	25	5.37
Ver. β_y	[mm]	0.7	0.85
Hor. α_x		0	1.75
Ver. α_y		0	0.89
Hor. beam size σ_x	[nm]	845	828
Ver. beam size σ_y	[nm]	19	28
Mean energy loss δ	%	0	2.59

Table 1: Beam TESLA parameters at IP.

When the spent electrons having an increased momentum spread pass through the strong focusing final doublet of the incoming beam a significant chromatic aberration appears there and an essential dispersion arises when they pass through the bending elements. The consequences of this are: it is very difficult to get the necessary beam sizes in the wiggler and accordingly of the γ-radiation spot on the conversion target, there are big problems to ensure 100%, i.e. loss-free capture of the spent beam in the channel. These circumstances oblige to undertake special steps to decrease as far as possible the influence of the chromatic aberration and of the dispersion on the beam dimension. On the other hand, during the accelerator commissioning and the tuning phases the dump can be destroyed because of the high power density deposited in it by the non-colliding low emittance and small size beams. To exclude this a special scanning magnets must be foreseen to sweep the beam on the dump surface.

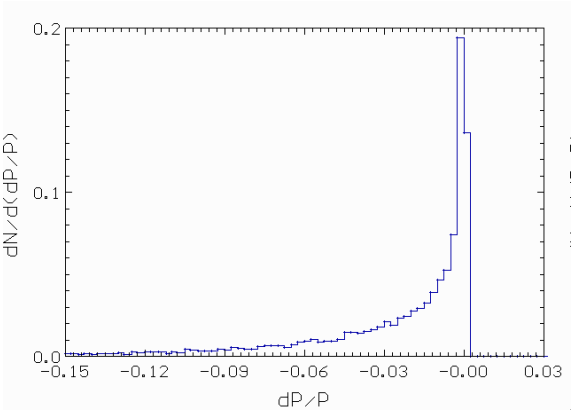

Fig.3: Momentum spent beam particles distribution in IP.

At the designing of the channel for the spent beam there should be solved few basic tasks. It is necessary: to separate the incoming to IP positrons and the outgoing electrons without the influence on the positrons, to get the necessary size of the electron beam in the wiggler to ensure the required sizes of γ-beam on the conversion target, to receive the desirable distribution of the beam on the dump, to incline the beam axis relative the earth surface at the dump by a gradient of 15 mrad. All these problems should be solved having as low as possible the beam losses along the channel. To fulfil these tasks we considered two possibilities. As one of them we chose the proposed in [1], [6] variant in which the traditional approach to compensate the chromatic aberration by sextupole lenses is used. In the second one we try to optimize the layout and the parameters of the channel elements to get the same or better results in a simpler way without using sextupoles.

THE SPENT ELECTRON BEAM LINE WITH CHROMATIC CORRECTION

The beam line structure

The modified spent electron beam line layout of the first variant is presented in Fig.4. Let's consider in more details its main parts and functions which they fulfil.

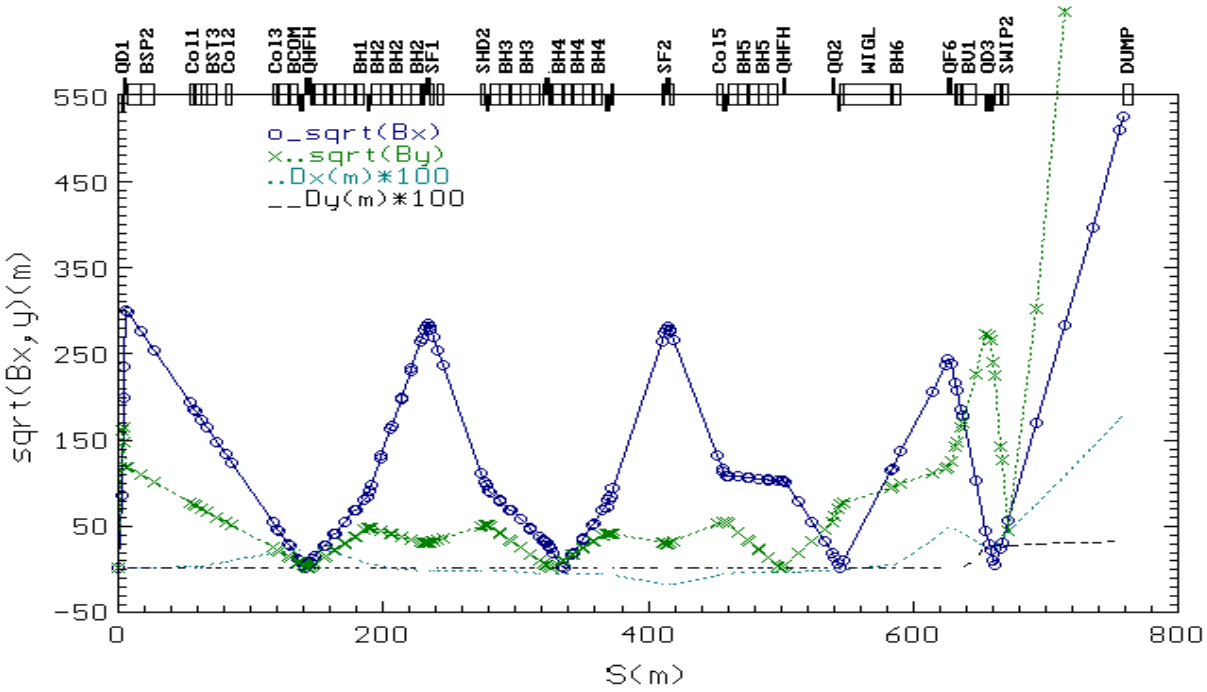

Fig.4. The layout and parameters of the electron beam line.

The incoming positrons and the outgoing spent electrons are separated by a extraction system, which is developed and described earlier in Ref. [7]. It consists of an electrostatic / electromagnetic separator and of three modules of septum - magnets. Because the horizontal emittance of the spent beam is more bigger than the vertical one the extraction is done in the horizontal plane. It is reasonable to avoid the additional increasing of the vertical beam dimension in the wiggler to conserve as small as possible its vertical aperture to orientate its field lines along this direction.

As the chromatic aberration arisen in the final focusing doublet of the incoming positron beam cannot be compensated in the place of its origin it is done in the horizontal plane by a chromaticity correction section (in the vertical plane it is not required because of the much smaller spent beam emittance). The chromaticity correction section consists of four FODO periods with a phase advance in each of them 90^0. Near to the focusing in horizontal plane quadrupoles in the second and in the forth FODO periods the compensating sextupoles are located. The phase advance between the main sextupoles is equal to π what allows to compensate the geometrical aberration [8]. In addition to the main sextupoles some ones are foreseen to optimize the energy bandwidth of the system [9].

To get the necessary sizes and divergence of the beam in the wiggler and, consequently the appropriate cross-section of the γ-radiation spot on the conversion target between the achromatic section and the wiggler a focusing module consisting of a quadrupole and a final doublet is foreseen. After the electrons are used to generate the γ-radiation in the wiggler they must be deflected to exclude the target hitting. The separation is carried out by the vertical bend magnet BV1. Creating a deflection of 15 mrad of the electron beam we get the muon beam emerging from the dump downwards away from the surface with the necessary gradient. To prevent the possible overheating of the water dump by the non-colliding beam it should be distributed uniformly on an area not less than 30 cm^2. The radius of the localized beam spot should be more than 0.1 mm. For this reason between the BV1 and the dump two 10 m long high frequency kicker magnets are installed. As each of them provide a beam sweeping along one of the transverse coordinate and their fields are phase shifted by 90^0, the beam on the dump describes a circle of 3 cm radius, large enough for the temperature rise in the dump water not exceed the allowable limit 80^0 C [2].

BEAM PARAMETERS

Taking into account the complicated spent beam particles distribution on the transverse phase planes we used for the definition of the beam parameters along the channel the matrix method calculation of the particles motion and apply the relations (1) to estimate the statistical parameters. For the particles tracing

the simulation codes "TRANSPORT" and "SCAPER" [10] are used. The particle trajectories were calculated taking into account the influence of the synchrotron radiation arising at its passage through electromagnetic elements. The beam transport efficiency from IP up to the wiggler is higher if the nominal channel energy is putted equal to 242.5 GeV what makes approximately the average particles energy after the interaction.

The γ-beam size on the target should not be more than 0.7 mm. It is determined by two main components: by the map size of the electron beam on the conversion target and by the natural angular divergence of the generated radiation. If consider them statistically independent and approximately equal the size of the beam map on the target should not exceed 0.5 mm. To ensure this requirement in the vertical plane there are no problems because, as the data of Table 1 show after the collision in this plane the beam emittance is two orders of magnitude less than in the horizontal plane. This is the reason, why we shall pay the main attention to the horizontal plane. Though the choice of the structure of the chromaticity correction system is rather simple the definition of the sextupoles strength is not so obvious. For the beam sizes minimization the following approach was chosen. On the conversion target an area of asize about 1.5 mm was set for the image beam projection. For the case when the fields in the wiggler and in the bending magnet behind it were zero the coordinate descent method was used to define the lenses strength at which the intensity in above chosen area on the target is at most. At these strengths all statistical parameters of the beam are calculated.

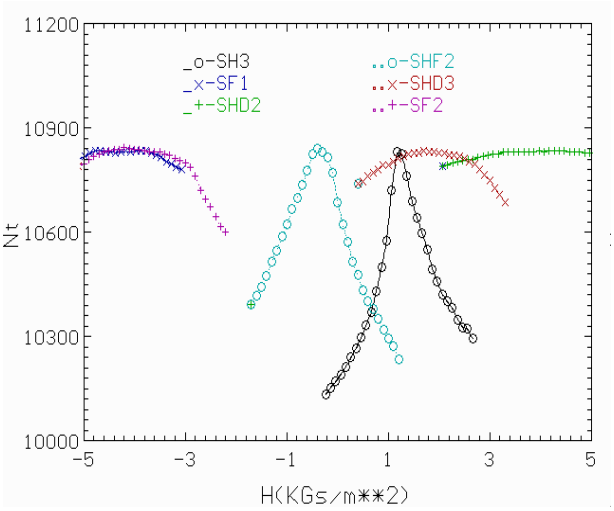

Fig.5: Beam intensity at the target as a function of sextupole lenses strengths.

In Fig.5 the dependence of the channel transport efficiency from IP up to the wiggler is presented versus the sextupoles strength. The maximum value of the efficiency is about 91%. As it is clear from Fig.5 the efficiency is most sensitive to the strength of the lenses in the first and the third FODO periods.

In the same way and with the same purpose some optimization of the strengths and of the arrangement of the quadrupole lenses was made. In Table 2 the dependence of the IP-wiggler line part transport efficiency versus the channel aperture size is given. One can see that the increase of the horizontal half-aperture up to36 mm reduces the beam losses on 3 %, whereas its further increasing is not effective.

A_x, mm	24	30	36	42
I, %	88	90	91	91.6

Table 2:The changing of the IP-wiggler transport efficiency (A_y=24 mm).

The changing along the beam line of the β-function and of the dispersion in Fig.4 and of the matrix elements in Fig.6 are shown in both transverse planes.

These data are got taking into account the results of the optimization procedures. The characteristics of the imaginary beam on the target and of the real beam on the dump entrance are presented in Table 3 for the follows collider operation modes:

- a normal beams collision mode (1),
- only electrons acceleration, without collision (2).

	Units	Target (1)	Dump (1)	Dump (2)
Hor. Emittance ε_x	[10^{-9}m]	7.6	79	7.4
Ver. Emittance ε_y	[10^{-9}m]	0.5	300	10.7
Hor. beam size σ_x	[mm]	0.18	28	5.8
Ver. beam size σ_y	[mm]	0.24	17	2.4
Mean energy E	GeV	237.4	235.0	238.7
Intensity I	%		90.5	100

Table 3: TESLA beam parameters at the target and the dump.

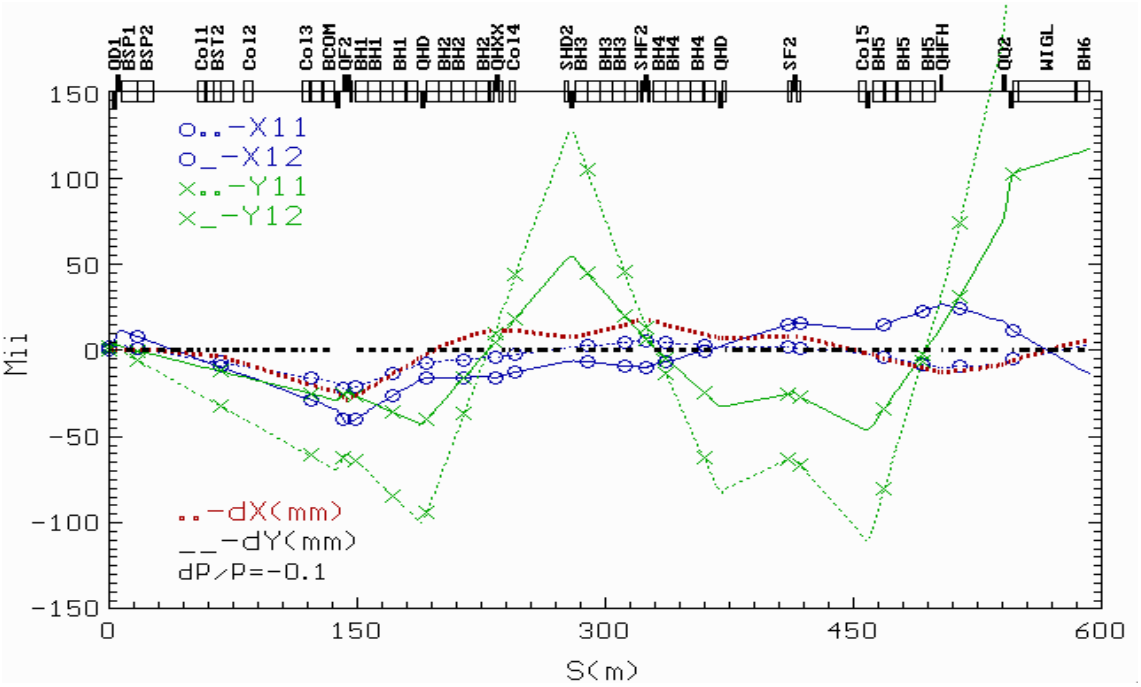

Fig.6: Matrix elements and displacement along the beam line.

Additional 0.5 % beam losses take place on the collimators to shield the wiggler (the efficiency in the Table is 90.5 % instead of the mentioned before 91%). It was necessary to intercept the particles which could hit the wiggler because of its restricted vertical aperture.

The natural γ-beam divergence can be approximately estimated as:

$$\sigma_\omega \approx \frac{eB\lambda_\omega}{2\pi p}\cdot\left(\frac{L}{2}+D\right), \quad (2)$$

where e, p are the charge and the momentum of the electrons, B, λ_ω, L are the magnetic field, the period length and the length of the wiggler accordingly, D is the distance between the wiggler and the target. If B = 1.7 T, L = 35 m, D = 30 m and λ_ω = 3.2 mm, as is foreseen in Ref. [1], σ_ω will be equal 0.5 mm. Taking into account this value and the dimension of the imaginary beam on the target we can conclude that the sizes of the γ-spot on the conversion target are within the required limits and the necessary positron beam emittance is provided.

In above considered modes the beam on the dump has certainly essentially different dimensions. In Fig.7 and 8 the beam distributions on the dump are shown in the transverse plane for the cases when the collision happens and without it. The integral of every distribution is equal to the total beam intensity. The beam size in the first case is approximately an order more than in the second one. It means that just the last regime is the most critical one for the dump.

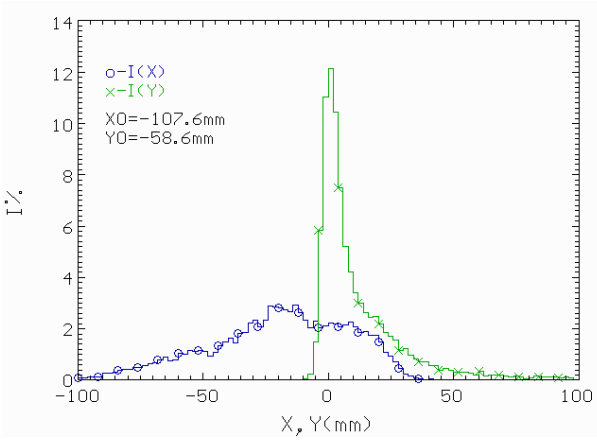

Fig.7: Distribution of colliding e^- at the dump.

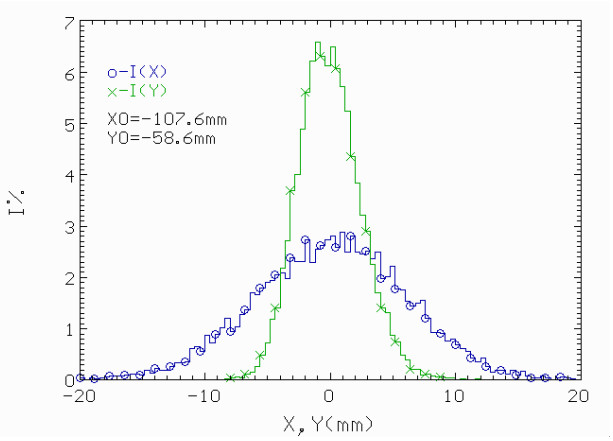

Fig.8: Distribution of e^- at the dump without collisions.

BEAM COLLIMATION

Because of the impossibility to capture in the beam line 100 % of the spent electrons it is necessary to provide a system of collimators to protect the equipment of the collider against the hitting of lost the particles. The following requirements must be satisfied at the collimators layout choice:

- the collimators should intercept only those particles which cannot be captured by the beam line,
- the collimators should protect the equipment from the direct hitting of the high energy electrons,
- to avoid the thermal overheating the maximal intensity intercepted by one collimator jaw should not exceed 2 % of the nominal collider intensity.

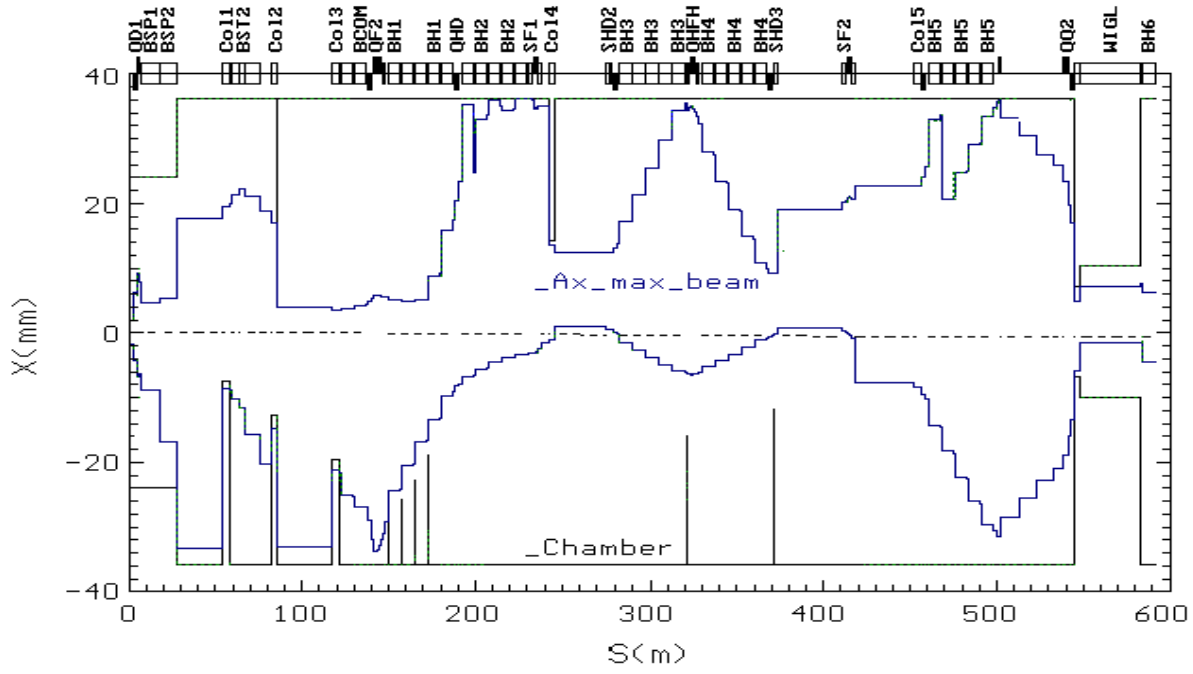

Fig.9: Electron beam envelopes in the horizontal plane.

Bear in the mind that the beam in the IP has small sizes and dispersion, the motion of the particles along the channel can be described by the relation:

$$x \approx \sqrt{\beta\beta_0} \cdot \sin\Delta\psi \cdot x_0' + \eta \cdot \delta_0 . \quad (3)$$

Where: x and x_o' are the coordinates of the particles on the phase plane, β_0 and β are the amplitude function of the particles in the initial and current points, $\Delta\psi$ is the phase advance of the particles oscillation, η and $\delta_0 = \Delta p/p$ are the dispersion and the momentum deviation of the particles. This expression is valid for both transverse planes, but for the vertical one $\eta = 0$ because there are no deflections in this plane. From (3) it follows that to intercept the particles with some momentum deviation it is better to put the collimators in the position where the dispersion has a considerable value, whereas the particles with a large initial angles deviation is more effective to intercept in the places, where β is close to a maximum and $\Delta\psi \sim \pi/2 + n$. But because of the high momentum spread of the particles theirs motion significantly differs comparing with the linear approach described by relation (3) and therefore the collimators arrangement made from this approach can be considered only as a rough approximation. The exact choice of their position should be carried out only on the base of the numerical account of the particle trajectories for the different momentum and for the various initial coordinates on the phase plane.

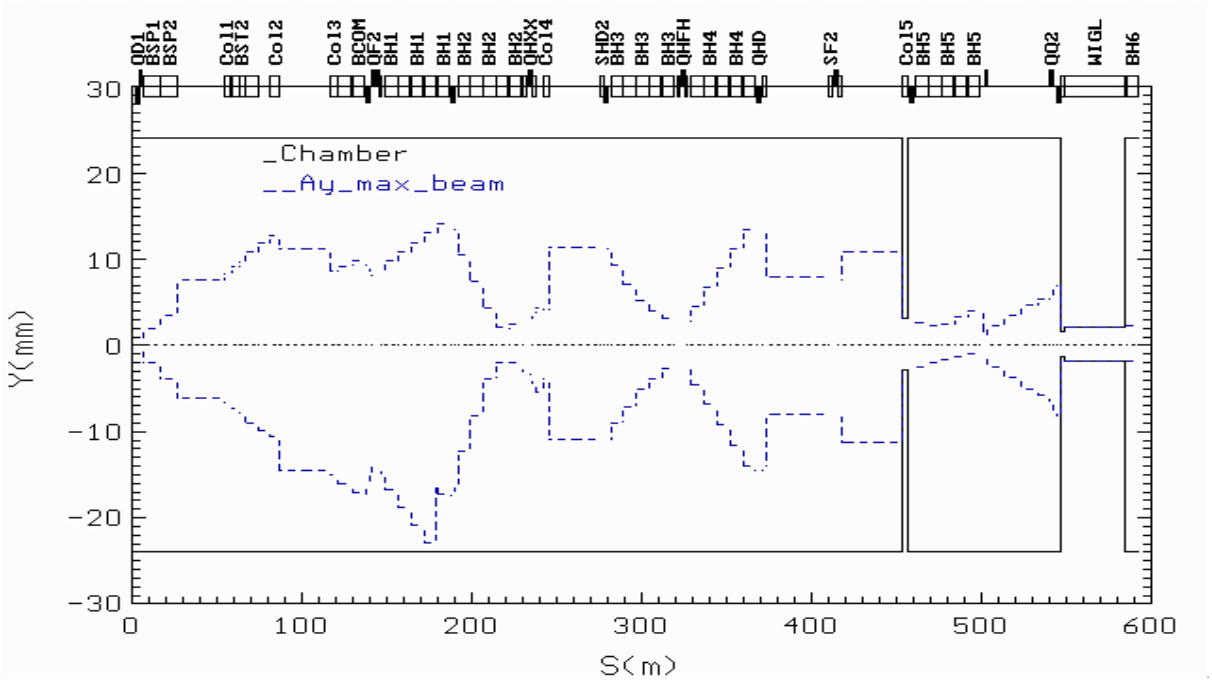

Fig.10: Electron beam envelope in vertical plane.

In Fig.9, 10 the beam envelops got by the computer simulation and in Fig.10 the collimators disposition in the channel are plotted. Fig.11 shows the distribution of the beam losses along the channel with the collimators presence and without them. One can see the significant losses increasing in the places where the collimators are installed and their essential reducing on other parts. These pictures confirm that the first three collimators really intercept the main part of the particles with a large momentum deviation, whereas the particles with the increased angular deviations are caught by the fourth and fifth once. The first collimator is split up into three parts in order to have a losses level per collimator not more then 2 % of the total beam intensity. The rough estimations show (more detailed accounts will be carried out somewhere later) that the excess of the specified limit can cause an inadmissible overheating and a destruction of the collimators. Taking into account the small vertical wiggler aperture a collimator is placed direct in the front of it to protect it against the hitting by the particles having here a large oscillation amplitudes. It is necessary to note that the given distributions have been got in the assumption that all particles that hit the collimator are absorbed in it. Actually it is not quite correct, as some part of them and of secondaries can leave the collimator and be absorbed elsewhere. The more detailed research of the influence of this effect will be made somewhere further.

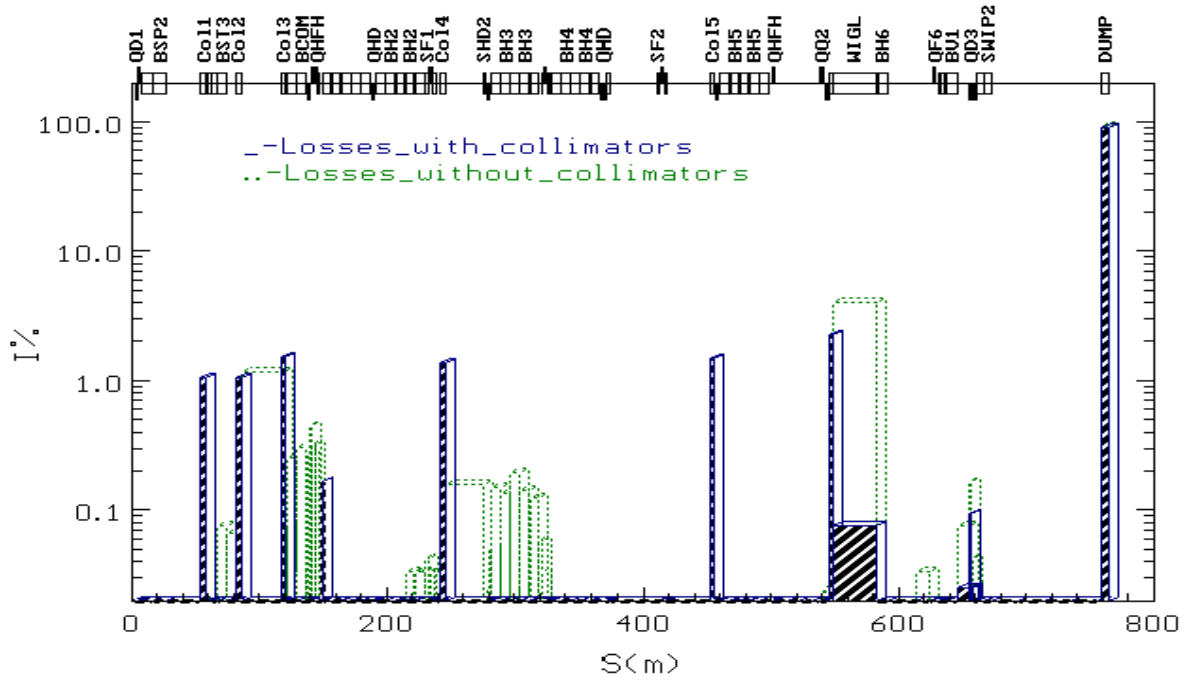

Fig.11: Distribution of electron losses with and without collimators.

It is clear that the instantaneous temperature in the collimator volume depends not only upon the total deposited beam intensity, but it is very important how the particles are distributed on the upstream surface of the collimator. These dates are presented for all collimators in Figs.12, 13,14.

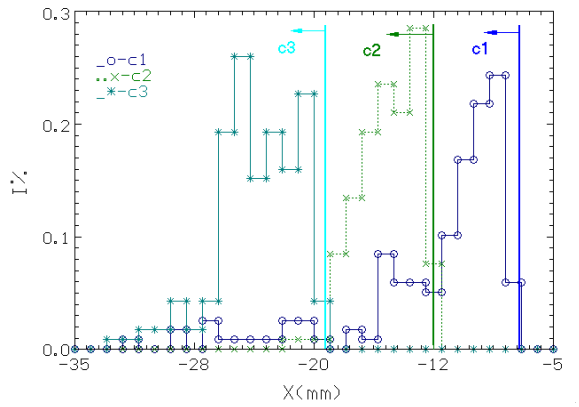

Fig.12: Horizontal electron distribution on the collimators 1,2,3.

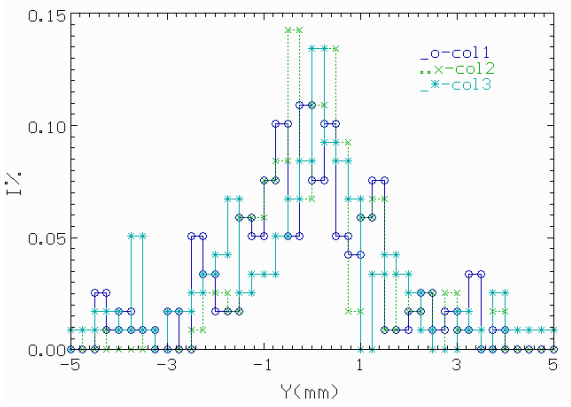

Fig.13: Vertical electron distribution on the collimators 1,2,3.

By the chosen channel structures and the electromagnetic characteristics of their elements the necessary beam parameters on the dump can be provided. The achieved electron beam dimension in the wiggler allows to get the required γ-beam size on the conversion target and accordingly the emittance of the positron beam. The electrons transport efficiency from the IP to the wiggler is about 91 % that guarantees the necessary positrons intensity. But there are inevitable 9 % of the beam which cannot be captured and transported in the area that is suitable for the γ-radiation and which lie outside of the wiggler aperture. All attempts to lower the number of these particles were without success. That is why the chromatic system works very well, when the momentum deviation of the particles $\Delta p/p$ is less than 5 %. Outside of this area

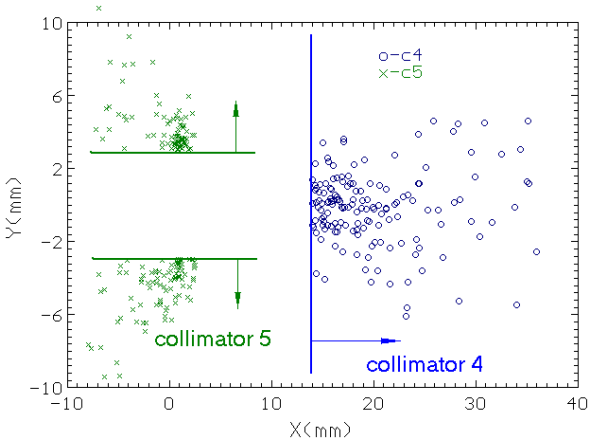

Fig.14: Phase plane on collimators 4, 5.

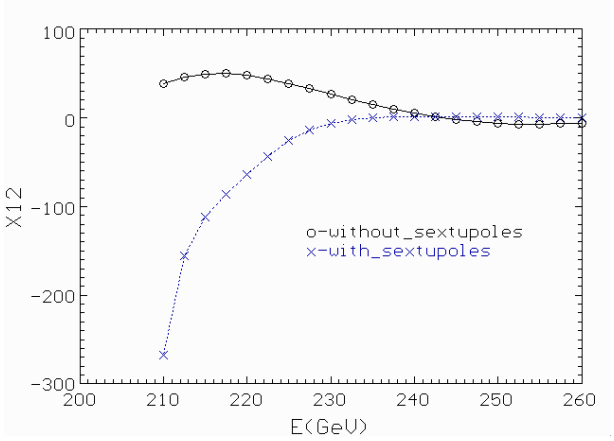

Fig.15: Matrix element X12 at the target versus energy.

the matrix elements and the dispersion change very nonlinear with the momentum deviation changing . This conclusion can be confirmed by the Fig.15, where for a comparison, the changing of the matrix elements X12 as a function of $\Delta p/p$ are presented for the cases when a chromatic correction is used and without it. One can see that as the energy becomes less than 220 GeV X12 changes more essential in the first case than in the second one. That part of beam, which cannot be captured for the transporting in the line must be intercepted by the collimators distributed along the channel from IP to the wiggler, what can be a very serious problem from the radiation protection point of view. This was the reason why we try to design a beam line without a chromatic correction system.

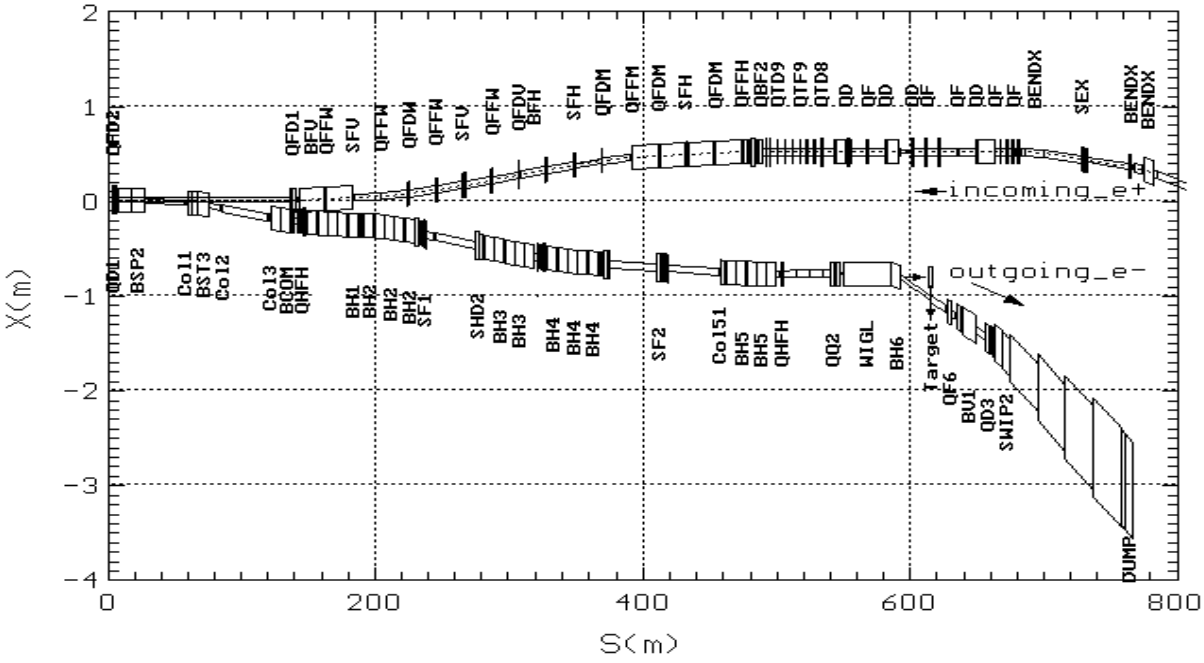

Fig.16: The plan of electron beam line.

The common layout of the channel and the disposition of its elements relative to the delivery system of the incoming to IP positrons are shown in Fig.16.

THE SPENT ELECTRON BEAM LINE WITHOUT CHROMATIC CORRECTION

Because the using of the chromatic correction system turns out to be not enough effective in the case of high particles momentum spread we solved to refuse it and try to simplify, as far as possible the channel

structure, but optimize more carefully the elements layout and its parameters. The goal was to get the same as in the previous case main beam date, i.e. the necessary spent and not colliding beam sizes in the wiggler and on the dump, but reduce essentially the beam losses. The layout of the simplified channel structure version and the main Twiss parameters are shown in Fig.17.

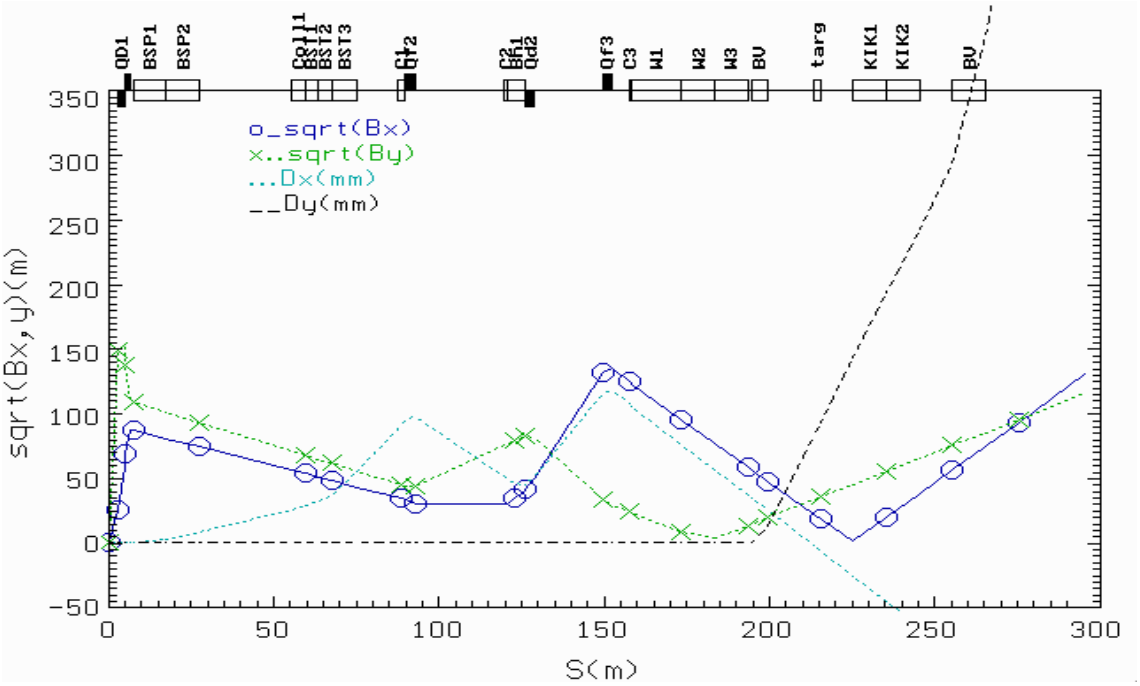

Fig.17: β–functions and dispersion in the electron beam line.

The separation of the incoming to IP positrons and outgoing electrons is executed by the same ejection system as in the previous variant. To reduce the influence on the beam size in the channel of the dispersion created by the ejection system bending elements the first focusing lens of the line should be installed as close as possible to the last ejection element. In Table 4 the dependence of the beam transport efficiency of the channel is presented as a function of the lens coordinate relative IP.

L_{IP},m	I%	I_t %	I(wiggler)%	σ_x	σ_y	L,m
75	97.87	87.49	0.546	0.546	0.061	201
90	***96.87***	***87.12***	***0.34***	***0.57***	***0.067***	***217***
105	95.67	91.00	0.33	0.67	0.066	235
120	93.9	90.93	0.27	0.65	0.064	251
135	***93.02***	***89.94***	***0.27***	***0.706***	***0.063***	***265***
150	92.5	88.68	0.36	0.82	0.060	280
165	***91.75***	***87.57***	***0.40***	***0.87***	***0.064***	***295***

Table: 4 Beam line parameters versus first lens coordinate.

Taking into account that the lens should not be hitted by the beamstrahlung coming from IP this distance can not be less than 90 m and the lens should be executed as a septum-quadruple two poles of which looking to the radiation side are replaced by a magnetic mirror. Nearly the second lens a dipole magnet is located to compensate the dispersion in the wiggler position point. Due to the large spent beam particles momentum spread it cannot be done in the all energy band therefore we limited ourselves by the requirement to perform this condition for the maximum $(\Delta p/p) = 0.1$ because outside of this momentum spread there are less than 10 % of the beam (see Fig.3). Again, using the coordinate descent method we defined the lenses and the magnets position and the magnetic fields level in them for the case when the beam transport efficiency is close to the maximum. To reduce the specific energy deposition density the collimators must be installed in the positions, where in the appropriate plane the envelope has a maximum. Because of the small linear sizes and the significant angular spread of the spent particles after IP the beam

sizes along the channel mostly depend on the value of the matrix element M_{12}. It means that the collimators should be placed, where M_{12} has a maximum. In Fig.17 the changing along the optimized channel of the matrix element M_{12} and of the deviation caused by dispersion are given for ($\Delta p/p$) = - 0.1. The behavior of these curves shows that the first collimator intercepts in mainly low momentum particles and the second one the particles having large vertical angles. The third collimator is used for the wiggler protection.

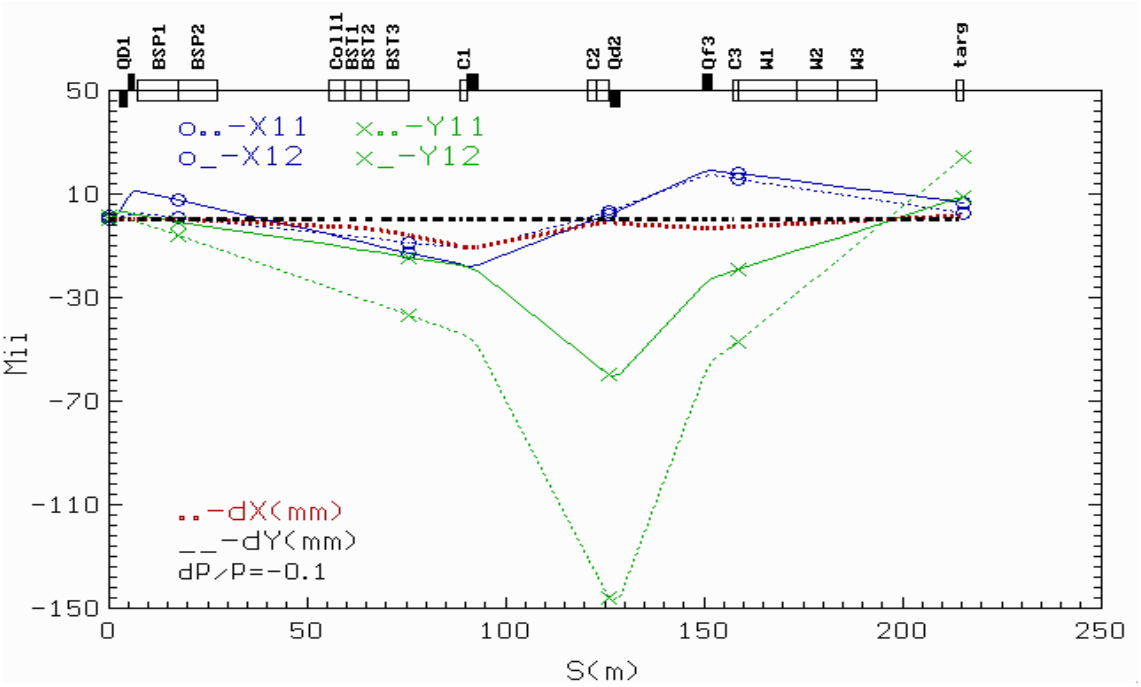

Fig.17: Matrix elements and displacement along the beam line.

As a result of the optimization we get the highest available beam transport efficiency of the channel. However, when there are some bottlenecks the distribution of losses between them is not quite obviously. So in our case, the collimator apertures and the vertical aperture of the wiggler are the bottlenecks. We should choose the apertures so that the main part of the particles which cannot be transported by the channel should be intercepted just by the collimator. To ensure this we map the collimator and wiggler apertures to IP using the defined matrix elements M_{12}. In IP they were put on the phase planes (Y,$\Delta p/p$), (X,$\Delta p/p$) together with the spent beam. Such drawings are shown in Fig.18, 19.

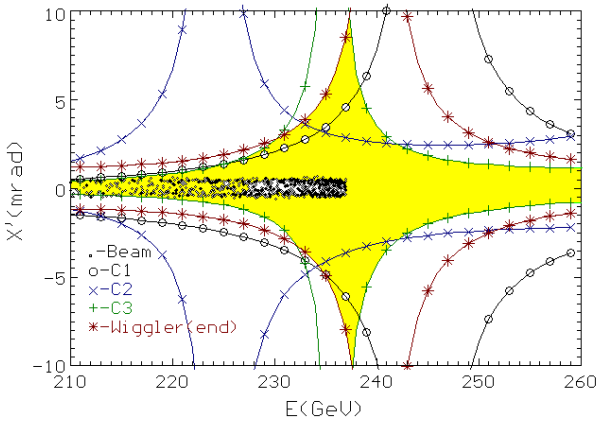

Fig.18: X',dP/P plane at the IP.

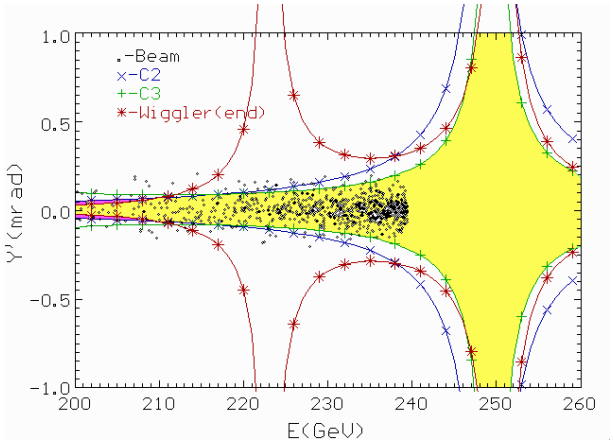

Fig.19: Y',dP/P plane at the IP.

If the apertures are chosen correct, the part of the plane displaying the external area of the wiggler aperture should be very few sparsely populated by particles, which are not intercepted by the collimator jaws. In

our case the higher available transport efficiency of 97 % was achieved when the number of such particles makes not more than 0.016 %.

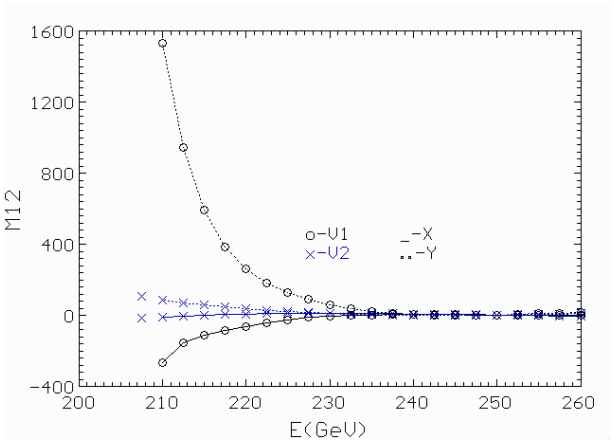

Fig.20: Matrix element M12 at the wiggler versus energy.

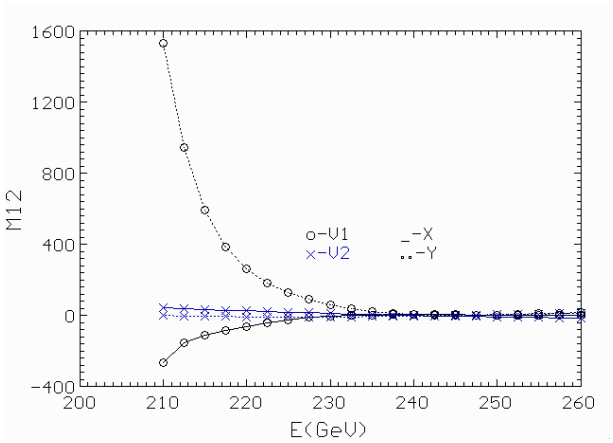

Fig.21: Matrix element M12 at the target versus energy.

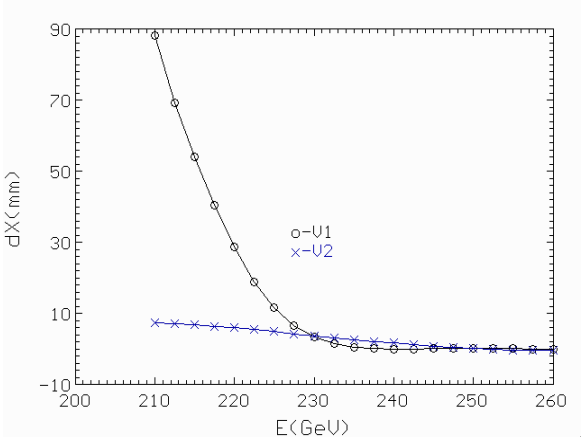

Fig.22: Displacement at the target versus energy.

In Fig.20-21 the changing of the matrix elements M_{12} on the wiggler input and on the conversion target are presented as a function of the energy. A similar dependence of the deviations caused by the dispersion on the target one can see in Fig.22. For the comparison, the same values of the variant with the chromatic correction system are drown there too (by V1 are signed the data of the variant with chromatic corrections system and by V2 without it). One can see the less energy dependence of the second variant parameters comparing the first one. This is the reason of the three times lower beam losses in the last version having also a simpler structure. In Table 5 the characteristics of the beam on the dump and it map on the conversion target are given for the colliding (1) and without collision (2) cases. The transverse particles distributions on the dump input for the specified modes are presented in Fig.23, 24.

	Units	Target(1)	Dump(1)	Dump(2)
Hor. beam size σ_x	[mm]	0.63	11	1.0
Ver. beam size σ_y	[mm]	0.17	46	6.5
Mean energy E	GeV	236.4	235.9	241.0
Intensity I	%	97	97	100

Table 5: TESLA beam parameters at the target and dump.

These data confirm that in both modes the necessary beam dimension on the dump and the spot size of the γ-radiation on the conversion target are provided if we take into account for the γ-radiation also its natural divergence. The distributions of the particles intercepted by the collimator jaw are displayed in Fig.25, 26.

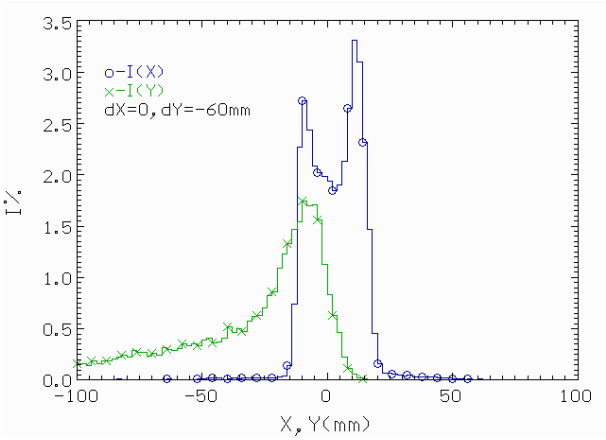

Fig. 23: Particles distribution of the colliding beam on the dump.

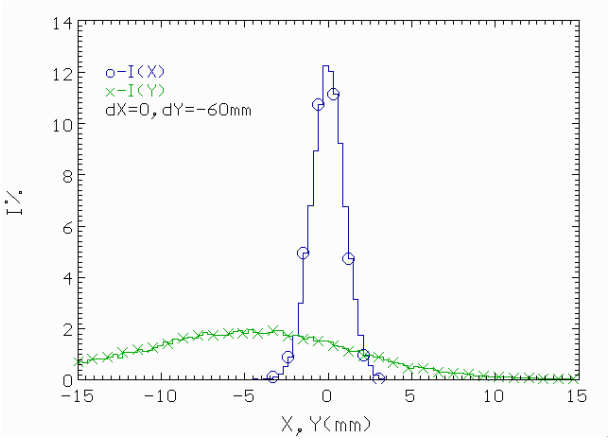

Fig. 24: Particles distribution of the beam without collisions on the dump.

It seems to be reasonable to make the detour of the conversion target in the vertical plane instead of the horizontal one as in the previous version. In this case the angular deviation created by the detour-bending magnet is only a part of the necessary total beam inclination in the vertical plane on the dump. The second

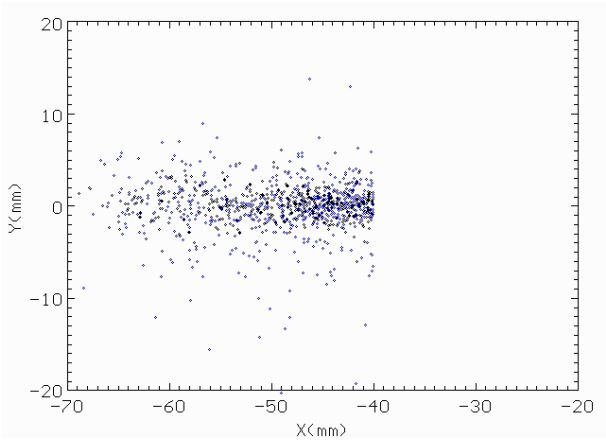

Fig.25: Phase plane at C1.

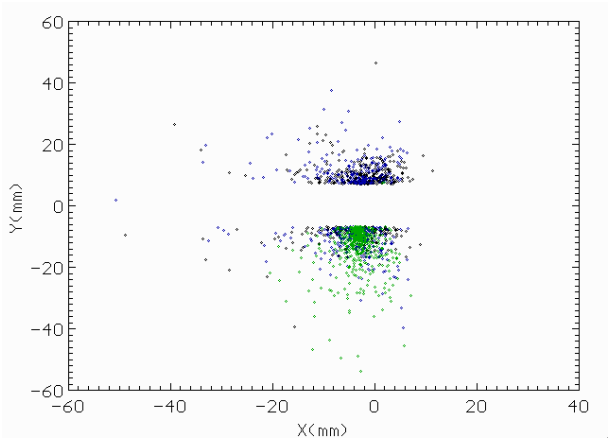

Fig.26: Phase plane at C2.

profit of this solution is that we exclude the essential additional increase of the spent beam size on the dump in the horizontal plane because of the dispersion, which could arise in the horizontal bending magnet.

The changing of the beam envelope and the distribution of the losses along the channel are shown in Fig. 27, 28. It is visible that at the chosen channel structure and the element apertures the beam losses occur practically only where the collimator are placed, whereas on other parts there are no ones.

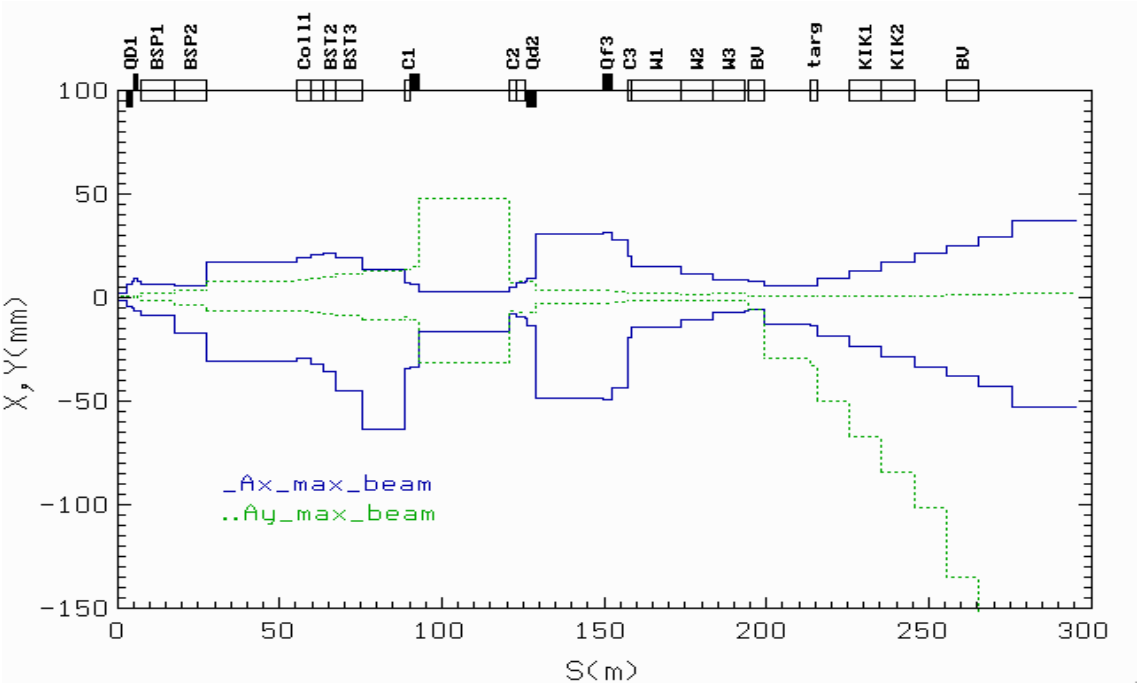

Fig.27: Electron beam envelope in the beam line.

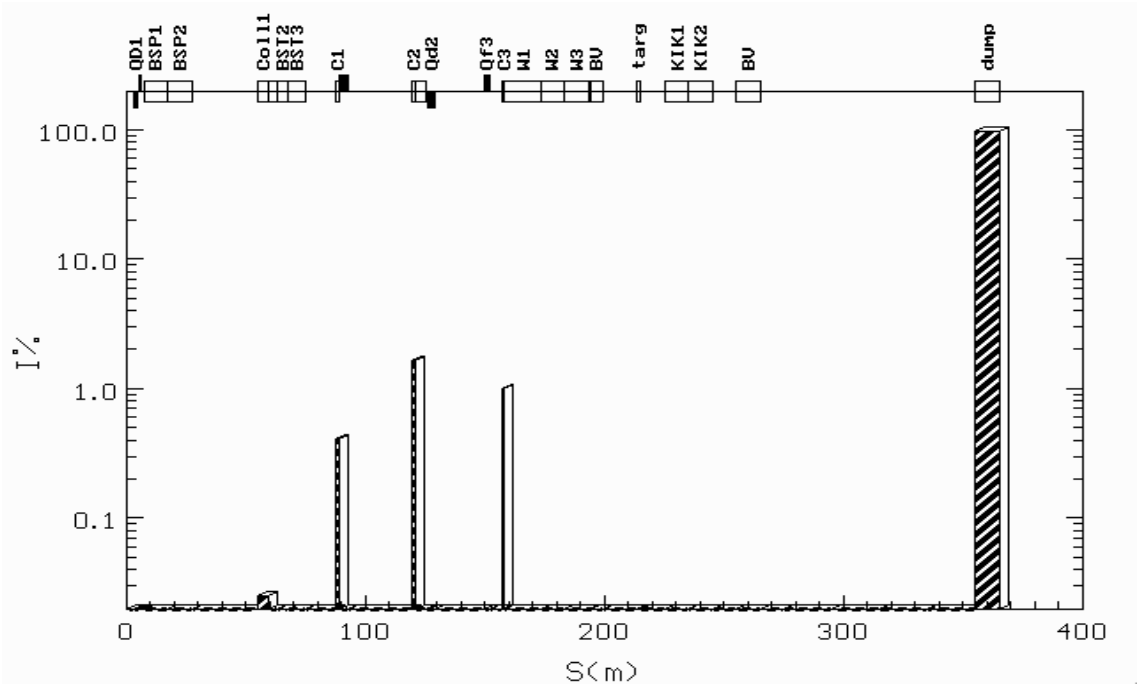

Fig.28: Distribution of the electron losses.

CONCLUSION

For the separation of incoming to IP and spent beams in the TESLA project an ejection system is used. Two possible channel layout for the capture and transport to the dump of the spent beam are discussed. A wiggler for the generation of γ-radiation which is together with a conversion target used as a positron source is in the lines foreseen. It is shown that in both layouts the necessary beam sizes on the dump can

be got to guarantee the tolerable temperature in it. The beam dimension in the wiggler ensuring required spot size of γ-radiation on the conversion target is provided. The achieved beam transport efficiency from IP up to the wiggler input 91 % in the first variant and, especially, 97 % in second one is more than enough to have the required positron intensity from the conversion target. The second variant of the channel structure seems to be more preferable from the radiation point of view because having also a more simpler structure the beam losses in it are three times less than in first one.

Acknowledgement

The authors would like to thank to Yu.Fedotov and Yu.Karshev for the useful discussion and the contribution to this work at the initial stage. A specially acknowledge to M.Maslov for his very detailed information concerning the required beam data for the water dump.

Bibliography

1. "Conceptual Design of a 500 GeV e^+e^- Linear Collider with Integrated X-ray Laser Facility", V1, DESY, 1997-048, May 1997.
2. M.A.Maslov, private communication.
3. K.Floettmann, "Investigations Toward the Development of Polarized and Unpolarized High Intensity Positron Sources for Linear Colliders", DESY, 93-161, 1993.
4. R.Brinkmann, Presented at LC92, EFCA Workshop on e^+e^- Colliders, Garmisch Partenkirchen, 25.7. -2.8.1992, EFCA 93-54.
5. P.M.Lapostolle, IEEE Trans. Nucl. Sci. No 3, 1101(1971).
6. R.Glantz, "A Feasibility Study of High Intensity Positron Sources for the S-Band and TESLA Linear Colliders", DESY, 97-201, 1997
7. A.Drozhdin, "Extraction of the Spent Beam into the TESLA Beam Capture Section", DESY, 1994, TESLA 94-29.
8. K.L.Brown, R.V.Servranckx, Proc. 11th Int'l Conf. On High Energy Accelerators, (Birkh"auser, Basel 1980).
9. R.Brinkmann, "Optimization of a Final Focus System for Large Momentum Bandwidth", DESY, M90-14, 1990.
10. I.I.Degtyarev, A.E.Lokhovitsky, Yu.S.Fedotov, I.A.Yazynin. "Integrated version of IHEP code system SCRAPER", VI Russian scientific conference on radiation shielding of nuclear installation. Obninsk, Russia, 1994.